

DEVELOPMENT OF A STANDARD APPROACH FOR WIND TURBINE MEASUREMENTS WITH AN ACOUSTIC CAMERA FOR OPTIMISATION PURPOSES

Sebastian Kümmritz

Ali Movahed

Johannes Pehe

gfai tech GmbH, Germany

kuemmritz@gfaitech.de

ABSTRACT

The air flow at the rotor blades causes turbulence which generates sound at the trailing edge of the blade. So-called serrations at the end edge of rotor blades break the turbulence into smaller structures, which shifts the sound emissions to higher frequencies. Simple sound pressure measurements can be performed to check the effectiveness of these serrations. However, sound pressure measurements with single microphones provide only integral values about the overall sound emission. In contrast, beamforming methods allow to determine the location of sound sources on the blade and an estimation of the amplitude of these sources. Therefore, the acoustic camera is an interesting analysis tool for the optimisation process of wind turbines, for example to determine the best position for the serrations. So far, no standardised approach exists for measurements on wind turbines with acoustic cameras. To develop such an approach, a measurement campaign with two different microphone arrays was carried out on two different wind turbines over a period of three days. The goal was to analyse the blade noise regarding to the distance and the azimuth angle between the acoustic camera and the wind turbine. Also the influence of downstream and upstream measurement positions was analysed. The results of these investigations will be discussed in order to establish a standard protocol for wind turbine measurements with acoustic cameras.

1. INTRODUCTION

Aerodynamic noise is a major health issue for the people living close to wind farms [1] which generates from the rotating movement of wind turbine blades and their interaction with the air which produces a swishing sound [2]. The noise emitted by a wind turbine must comply with specific regulations and limits, depending on the place where the wind turbine is operated [3]. To reduce this aerodynamic noise, it is crucial to investigate the acoustical characteristics of wind turbine.

Single-microphone methods only provide information about the overall noise and not on the location and intensity of the source. On the other hand, acoustic cameras are being widely used in order to localise sound sources using beamforming algorithms [4]. An acoustic camera consists

of a group of omnidirectional microphones arranged in a specific configuration. The configuration and the size of the microphone array defines the frequency range for the localisation of the sound sources. The signals picked up by the microphones are delayed and summed in order to interfere constructively [5].

In this study, we used an acoustic camera consisting of 48 microphones on three arms to measure noise emissions and investigate the influence of using serrations at the rotor blades. The large array diameter of 3.4 m makes it possible to localise low frequencies for outdoor applications. In addition, measurements with an array of 120 microphones arranged in a spiral configuration with a diameter of 0.95 meters were used for comparison. The measurements took place at the citizen wind farm Janneby between the 25th and 27th of October 2019. Two different wind turbines were investigated, one with and one without serrations.

The aim of this work was to develop a systematic approach to investigate the noise emissions at the blades with an acoustic camera. This can help to better assess the effectiveness of measures to reduce sound emission, such as the installation of serrations.

2. THEORY

2.1 Beamforming

2.1.1 Algorithm

The basis of sound source localisation using beamforming algorithms is the analysis and processing of runtime and phase differences between the sound sources and single microphones of the array respectively. For simplified view only stationary sources are considered. The principle is based on a mathematical compensation of runtime differences of the noise signal from any point x in an image plane to the single array microphones. The calculation of the reconstructed time waveform of the sound pressure $\hat{p}(x, t)$ for a location $x = (x', y', z')^T$ in the image plane is carried out by using the so called delay-and-sum algorithm:

$$\hat{p}(x, t) = \frac{1}{M} \sum_{i=1}^M f_i(t + \Delta_i) \quad (1)$$

where t is the time, M the number of microphones in the array, f_i the sound pressure time waveform recorded by

the microphones at position x_i (see for example [5]). The relative runtime difference Δ_i is derived from the absolute runtime τ_i , which are calculated for each microphone as $\Delta_i = \tau_i - \min(\tau_i)$. The absolute runtime $\tau_i = |r_i|/c$, with c the speed of sound in air ($c = 344$ m/s at 20 °C) and $|r_i| = |x_i - x|$ the geometric distance from microphone i to a point x . Equation 1 is solved for any point of a defined image plane. A time waveform is calculated for each pixel and the rms or maximum value can be displayed as color coded levels. This representation is typically referred to as an acoustic map. The superposition with a photographic image displays the position of dominant sound sources and is called acoustic photo.

2.1.2 Dynamic range and main lobe width

Two fundamental properties to describe the quality of a beamforming result are the main lobe width and the dynamic range. They are mainly determined by the array design and the frequency of the investigated component.

Figure 1 shows the amplitude distribution of a simulated beamformed signal along one axis for a ring array with one central noise source. The maximum amplitude occurs at the source location. The amplitude does not decrease continuously with increasing distance to the source but shows a pattern of local minima and maxima.

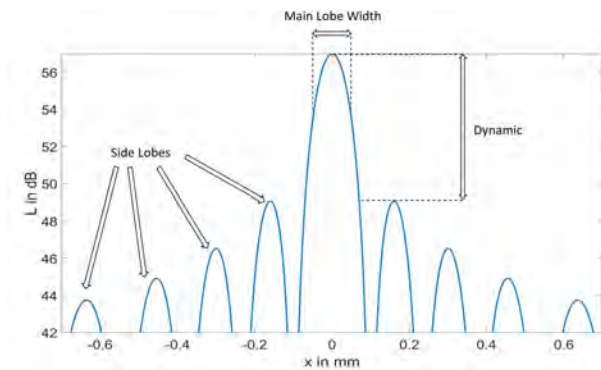


Figure 1: Amplitude of a simulated, beamformed signal along one axis for a point source centrally located in front of the array

The amplitude difference between the maximum value of the main and the first side lobe represents the dynamic range. Multiple sources can only be located simultaneously with conventional beamforming algorithms if the level difference is lower than the dynamic range of the array.

The main lobe width is the distance where the amplitude of the beamformed signal has dropped by 3 dB compared to the maximum. It restricts the localisation of adjacent noise sources. If the main lobe is wider than the distance between the sources, neighbouring sources will appear as one source.

The width of the main lobe and possible dynamic ranges are determined by the array design. According to [6] spiral microphone setups provide the best compromise of low main lobe width and high dynamic range, which makes them widely applicable.

2.1.3 Acoustic photo

Acoustic photos can either be calculated in the time- or the frequency domain. Figure 2 displays an acoustic photo generated from the time domain data. It depicts the time waveforms of the 48 microphones on the top and the acoustic photo on the bottom. The timeframe marked in black corresponds to the time interval (integration time) for which the acoustic photo was calculated.

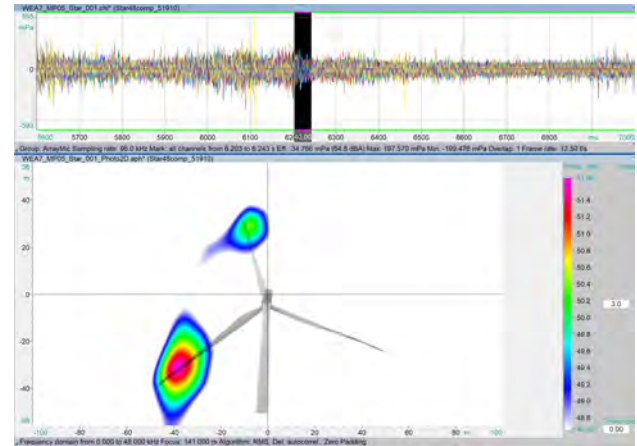


Figure 2: Acoustic photo generated from the time domain

Figure 3 illustrates the result of the frequency domain beamforming with the same integration time as in figure 2. The frequency spectrum calculated from the chosen time domain is shown on the top. In this spectrum the frequency range of the 1.25 kHz third octave band is marked. The acoustic photo on the bottom of figure 3 is calculated from these frequencies. For a better representation of the results, only the acoustic photos are usually shown in this paper.

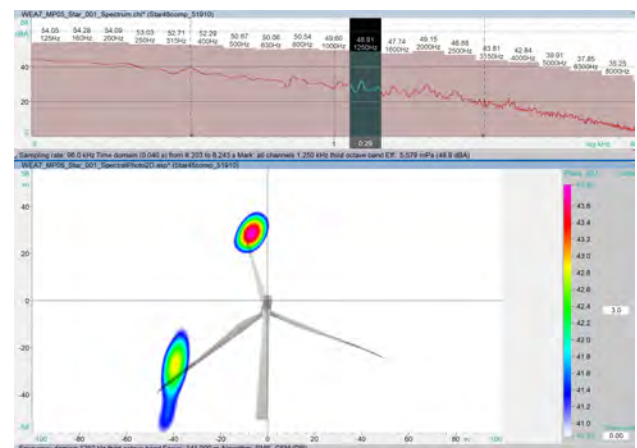


Figure 3: Acoustic photo generated from the frequency domain

2.1.4 Focus of the acoustic camera, rotation angle and focus dependent delay

Due to the different runtimes between light and acoustic it is necessary to compensate the delay (focus dependent

delay). Furthermore, it has to be considered, that the camera is pointing at the wind turbine hub at an angle, which causes a tilted focus plane. This is a potential source of error due to the fact that the focus distance is only accurate at the horizontal line where the camera focus plane cuts the rotor plane of the wind turbine. Figure 4 illustrates this, with the black area representing the focal plane and the grey area representing the rotor plane. The difference in distance from array to a blade tip might vary up to 50 metres at measurement distances close to the reference position. In order to compensate this error a computational focus plane rotation around the rotor centre was executed before the beamforming algorithm was applied.

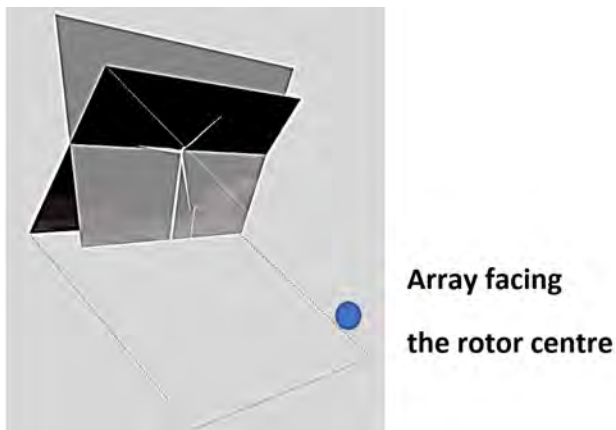


Figure 4: Focus (black) and rotor plane (grey)

2.2 Wind turbine noise

2.2.1 Theory

The noise emitted by an operating wind turbine can be divided into mechanical and aerodynamic noise. Mechanical noise originates from different machinery components, such as the generator and the gearbox. This noise propagates as structure-borne sound and is emitted via the structure as airborne sound. Aerodynamic noise is radiated from the blades and is caused by the interaction of turbulence with the blade surface. The turbulence can be originated either from atmospheric turbulence present in the incoming flow or from the viscous flow in the boundary layer around the blades. The focus of this paper lies on the investigation of aerodynamic noise, since nearly no mechanical noise was present during the measurements. A detailed overview of the theory of wind turbine noise can be found in [7].

2.2.2 Serrated wind turbine blade trailing edge

Among other implications on the engineering design of the wind turbine blade, the serrated wind turbine blade trailing edge is acoustically designed to reduce the noise induced by Karman vortex shedding. Figure 5 shows a schematic drawing taken from an european patent application [8]. Typically, reductions between one and three dB are possible. The blades of type LM58.7 used on the Vensys 120 are equipped with trailing edge serrations.

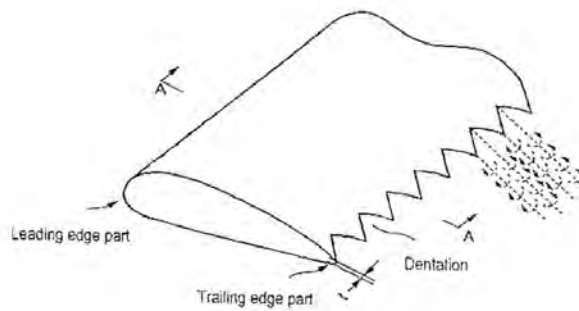


Figure 5: Schematic drawing of trailing edge serrations from [8]

2.2.3 Reference position

In order to fully characterise the noise emissions of a wind turbine the IEC 61400-11 provides a detailed measurement and analysis procedure [9]. The procedure is based on sound pressure measurements at one mandatory reference position at a distance R_0 from the wind turbine tower to the microphone. The position needs to be within $\pm 15^\circ$ of the downwind direction. For horizontal axis turbines R_0 is given by $R_0 = H + \frac{D}{2}$ where H is the vertical distance from the ground to the rotor centre and D is the diameter of the rotor with a 20% tolerance. This distance range has been used as a reference for the most presented tests.

3. MEASUREMENTS

3.1 Equipment

The measurements were performed with two microphone arrays of the company gfai tech. The first one, the Star48, is a 48 channel array designed for outdoor applications. It consists of three arms with 16 microphones each. The diameter of the array aperture is 3.4 meters. The array is suitable for the localisation of sound sources in the frequency range between 66 Hz and 13 kHz.

While the majority of testing were carried out using the Star48, the second microphone array, Fibonacci120, was used for a performance comparison. The Fibonacci120 consists of 120 spirally arranged microphones and has a diameter of 0.95 m. This array is suitable for sound source localisation in the frequency range between 262 Hz and 20 kHz.

For data acquisition the mcdRec of the gfai tech with a sampling rate up to 192 kS/s and a resolution of 32 bit was used. Figure 6 shows the whole measurement setup with both arrays.

3.2 Wind turbines

Two different wind turbines were investigated, one with and one without serrations. Technical details are summarised in table 1.



Figure 6: Picture of a full measurement setup consisting of both arrays, data acquisition system and computer

	Vensys 112	Vensys 120
Rotor diameter	112.5 m	119.9 m
Hub height	93.5 m	90.0 m
Nominal power	2.5 MW	3.0 MW
Blade type	LZ55	LM58.7
Serrations	no	yes
Clockwise rot. speed	12.75 rpm	13.6 rpm

Table 1: technical details of the investigated turbines

3.3 Measurement positions

For the investigation of the wind turbines, a large number of measurements were carried out at different positions in upwind and downwind direction. The distance to the turbines was varied as well as the angle. However, except from the comparison of upwind and downwind in section 4.3 and the comparison of relative source positions at different angles in section 4.5 mainly the measurement positions in downwind direction according to the reference positions were investigated. According to the plant data in table 1, the reference distances to the examined wind turbines are between 120 and 180 metres directly in front of the wind turbines.

4. RESULTS AND DISCUSSION

4.1 Integration time

First of all, the influence of the integration time on the acoustic maps has to be analysed. Since moving objects are investigated, a long integration time may lead to a blurred image of the acoustic sources. On the other hand, a short integration period leads to a poor frequency resolution for lower frequencies.

In figure 7 the acoustic photos of the wind turbine with different integration times are shown. From that view, the rotation direction is counterclockwise. The pins indicate the tip positions of the blades during the rotation. The measurement position was chosen in accordance to IEC 61400-11 [9]. The first picture is calculated for an integration time of 4.46 seconds, which corresponds to a full rotation of the blades. The acoustic emission is much louder when the blade is moving downwards than when it is moving up-

wards. Since it can be assumed that the sound power level is independent of the rotor position, a strong directional pattern can be concluded from this.

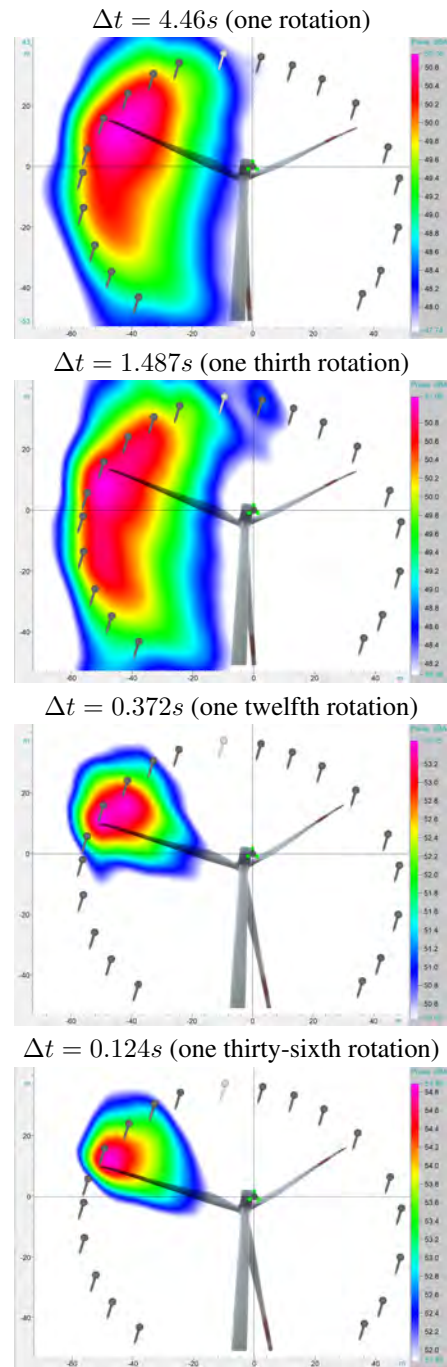


Figure 7: Acoustic pictures of the Vensys 112 from the time domain with different integration times

The second picture of figure 7 is calculated for an integration time of 1.487 seconds, which corresponds to a third rotation of the blades. The acoustic map looks nearly similar to the first one. A further reduction of the integration time leads to a smaller source representation. The third picture in figure 7 is calculated for an integration time of 372 ms. It shows clearly the emission of a single blade. The last picture shows the acoustic map for an integra-

tion time of 124 ms. The acoustic photo is qualitatively comparable to the previous one. However, the amplitude increases with decreasing integration time, provided the blade is at the loudest position of the revolution in the selected time range.

From the results it can be concluded that the integration time does not have to be chosen as small as possible to get a good sound source representation of the blades. The best integration time depends on the purpose of the investigation. For the identification of the rotor position with the loudest sound emission regarding to the measurement position, an integration time of about one revolution is suitable. To compare the effectiveness of constructive measures such as the installation of serrations, a short integration time of less than a twelfth of a revolution is useful, assuming comparable wind conditions for the different measurements. For some results in this paper very short integration times of about 40 ms were chosen, especially when transient effects were investigated.

4.2 Frequency foot prints

Beamforming enables to determine the time function of a source emitted from a specific point. This is comparable to the recording with a single microphone with strong directional pattern. To "hear" the blades on the position of the downwards movement, the time signal at the loudest point of an A-weighted acoustic map was extracted. The acoustic map was calculated with an integration time of 11.3 seconds (corresponding to two revolutions in this measurement). The top graph of figure 8 shows the time function of the sound pressure level $L_p(t)$ (window length: 125 ms) of the beamformed signal. Additionally, $L_p(t)$ of a single microphone is drawn in the graph. It can be seen that the beamformed signal is on average 18 dB quieter than the microphone signal, but the qualitative course is quite similar.

However, highpass filtering shows the improvement of the signal quality. The bottom graph of figure 8 shows the curves of the high-pass filtered sound pressure levels of both signals. In contrast to the filtered microphone signal the filtered beamformed signal shows clearly the individual passes of the blades at the listening position.

The technique of extracting the beamformed signals can be used for a detailed disussion of the influence of serrations. Therefore, the beamforming was applied to both wind turbines with an integration time corresponding to one revolution. Figure 9 shows the results. The left part of the figure shows the Vensys 112 (distance to the nacelle: 141 m, Wind speed: 11.5 m/s, rpm: 14.1, power: 2.55 MW) and the right part of the picture shows the Vensys 120 (distance to the nacelle: 138 m, Wind speed: 15.2 m/s, rpm: 13.0, power: 3.0 MW). First of all, one can see, that there is a noticeable difference between both turbines. The positions of the maximum sound emissions are slightly different and the range of the loudest sound emission is much larger for the Vensys 120. The latter could be explained by a less directional sound radiation caused by the serrations.

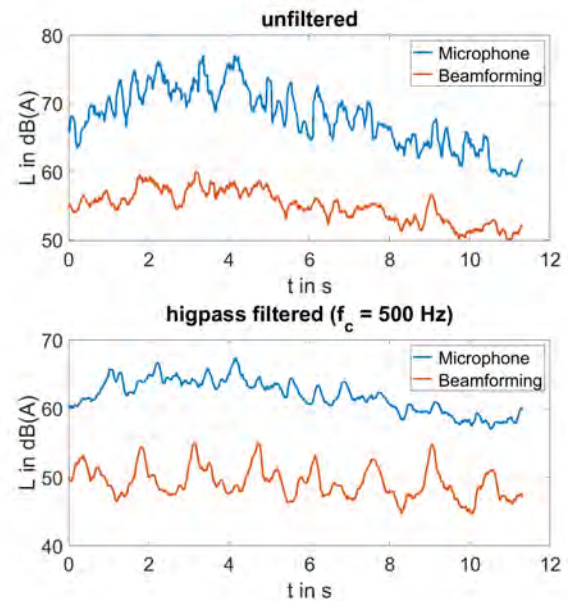


Figure 8: Time functions of the sound pressure level of a single microphone and a beamformed signal without (above) and with high pass filtering

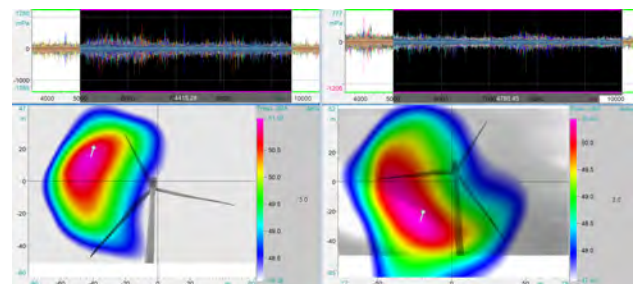


Figure 9: Beamforming results for both turbines (left: Vensys 112, right: Vensys 120) with an integration time corresponding to one revolution

For both turbines the time signals at the point of the loudest sound emission are extracted (marked in figure 9 by pins). Figure 10 shows the peak hold spectra of these beamformed signals. One can see that the sound emission of the Vensys 120 is in overall lower than that of the Vensys 112, although a higher wind speed was present during the measurement of the Vensys 120. Furthermore, a more flat frequency response in the region between 100 and 500 Hz can be seen. This effect is expected since the serrations break the turbulence into smaller structures. This shifts the sound emission at low frequencies to higher frequencies.

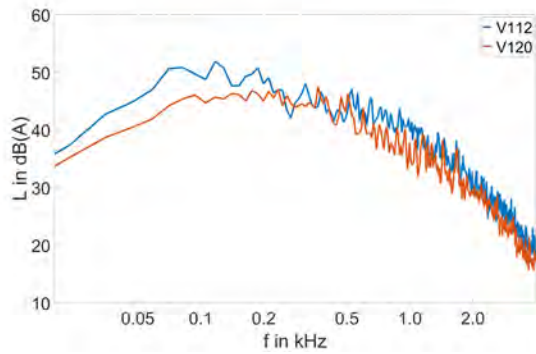


Figure 10: peak hold spectra of the beamformed signals at the loudest spot of both wind turbines

4.3 Upwind vs downwind

Figure 11 shows the results of the acoustic imaging of the Vensys 112 for up- and downwind measurement position. The distance to the nacelle was 151 m for the upwind and 141 m for the downwind measurement. The integration time corresponds in both cases to one revolution. Table 2 lists the measurement conditions during both measurements.

	upwind	downwind
distance to the nacelle	151 m	141 m
wind speed	12.7 m/s	11.5 m/s
rotation speed	13.5 rpm	14.1 rpm
power	2.51 MW	2.55 MW

Table 2: Measurement conditions for the upwind/downwind comparison

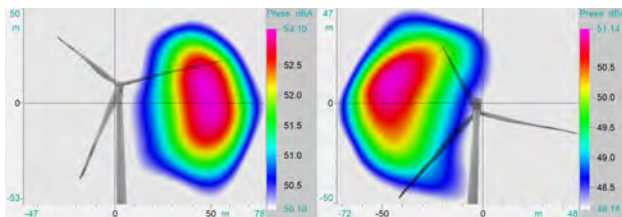


Figure 11: Comparison between upwind (left) and downwind (right) measurement position on the Vensys 112

The directivity appears similar. In the upwind case, the maximum sound pressure level is about 2 dB higher. However, the wind speed was a little higher compared to the downwind measurement. Also the rotational speed was a bit lower which causes a longer integration time and therefore a little higher sound pressure level.

We conclude that for the purpose of sound source localisation it makes no significant difference between upwind and downwind. The results indicate that higher sound pressures are measured at the upwind position, which may lead to a better SNR. The higher amplitude can also be caused by the flow of wind at the microphones of the array. In the upwind case, the signal noise caused by the wind flow is possibly a bit lower. On the other hand, since the quality of sound source localisation is not influenced by the measurement position, it might be advisable to choose the downwind position in accordance to IEC 61400-11 which enables a better comparability to acoustic data obtained by conventional measurements.

4.4 Transient effects

As it is shown in figure 12 on the emissions of different third octave bands for the Vensys 120, transient noise sources are visible. These sources appear on the turbine hub and occasionally on the full rotor. The events appeared only about 1 to 3 times during one rotation, determined with an integration time of 40 ms, and mostly occurred in the frequency range above 1 kHz. One event is shown in the 630 Hz third-octave band. These emissions are not significantly contributing to the overall noise emissions in this case and are presented for information only as they illustrate the approaches capability in terms of trouble shooting in case of rare unwanted effects. Audible transient noise emissions can have psychoacoustic impact as well.

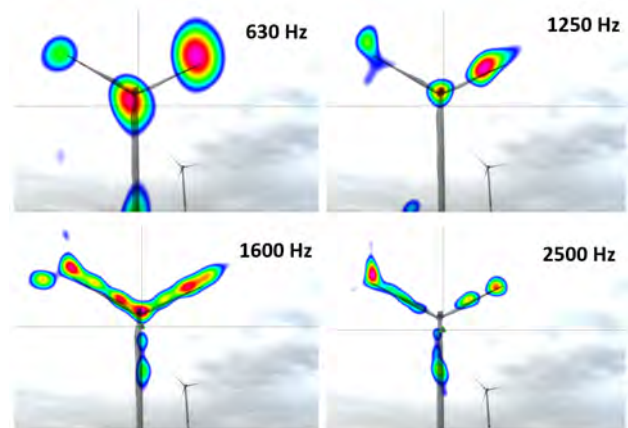


Figure 12: acoustic photos of transient effects found in single third-octave bands for Vensys 120 (integration time: 40 ms)

4.5 Relative source positions at different measurement angles

As it is of particular interest to evaluate the potential influence of serrations on the location of maximum sound

emission on the blades, the measurement positions are investigated comparing results obtained from different angles. Figure 9 showed a straight on view for both turbines. The dominant region of the sound emission was located during the downward movement of the blades next to the tips. However, the maximum sound radiation does not take place right at the tips but a bit shifted towards the nacelle.

Figure 13 shows the acoustic photos for measurements with an oblique view of the wind turbines from the left and right side (integration time corresponding to one revolution). In both cases it can again be seen that the main emission of the sound occurs during the downward movement of the blades. The main difference is that the sound emission appears further up at the left measuring position than at the right measuring position.

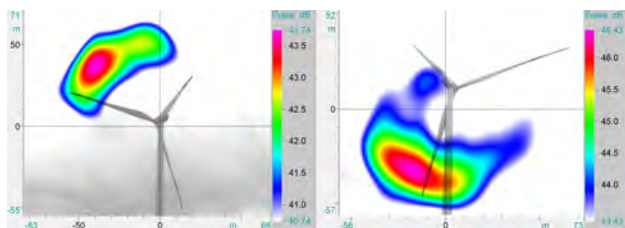


Figure 13: Comparison of the acoustic photos, calculated with an integration time of about one revolution, for different angles to the wind turbine (Vensys 112) in downwind position

During both measurements the wind conditions were similar with 14.9 m/s for the measurement from the left side and 15.1 m/s for the measurement from the right. The higher source amplitude of the measurement from the right can be explained by a smaller measurement distance. The distance to the nacelle for the measurement from the left was 196 metres and 154 metres for the measurement from the right.

These results show again the strong directivity of the sound emission caused by the blades. However, no additional information was obtained. From this it can be concluded that a measurement with a direct view to the wind power plant is preferable.

4.6 Comparison of array design

The Star48 is designed for long range measurements and the localisation of low frequencies. The array is lightweight and can be quickly assembled and disassembled in the field thanks to its foldable arms. However, this array geometry provides some drawbacks. The dynamic range is comparatively low and very characteristic side lobes can appear. This can be seen in figure 14 in a simulated acoustic map. For the simulation a wide band noise source in a distance of 100 metres was chosen.

In contrast, spiral arrays such as the Fibonacci120 are characterized by good dynamics. However, the microphone arrangement is more complicated, what results in a less simple and flexible setup and dismantling.

Figure 15 shows the comparison of a sound source localisation on a blade of the Vensys 112. Both pictures show

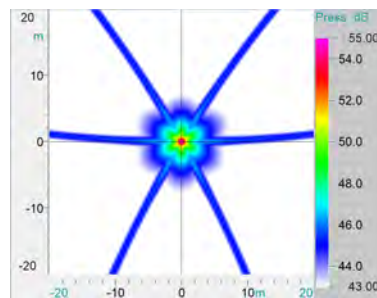


Figure 14: Array pattern of the Star48

the acoustic photos for the 1250 Hz third octave band with 12 dB dynamic (integration time 80 ms). The maximum amplitude is almost the same at 45.1 dB for the Fibonacci measurement and 44.7 dB for the Star48 measurement. However, there are very clear differences in the individual patterns. The main lobe for the Star48 measurement is much smaller than for the measurement with the Fibonacci, but noticeable side lobes appear. On the other hand, the diameter of the Fibonacci is significantly smaller, which is one reason for the significant larger main lobe width. The best practise would be a spiral array with the aperture size of the Star48.

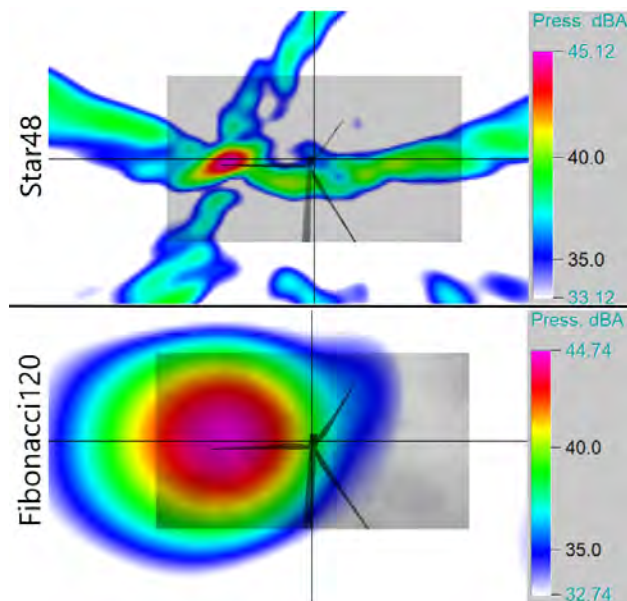


Figure 15: Comparison of the beamforming pattern of both arrays

5. SUMMARY

In this paper, we presented some aspects which help to develop a standard approach for noise localisation and optimisation on wind turbines by means of acoustic cameras. One microphone array consisting of 48 omnidirectional microphones with a star structure and a second array consisting of 120 microphones with a spiral array design were used to find the origin and sound pressure level of aerodynamic noise sources. The measurements were performed

with respect to different locations and directions from the wind turbine to the microphone array.

It was illustrated that an integration time of one revolution is optimal to find the loudest noise emission. The results showed that the downward movement of the blade is significantly louder than the upward movement, which is caused by a strong directional pattern. Observation of the frequency characteristics of the sound sources at the location of the loudest sound emission shows that the blades equipped with serrations are significantly quieter, especially at frequencies below 250 Hz (A-weighted). A comparison between upwind and downwind showed that the noise source location is similar but the upwind turbine is around 2 dB louder. Furthermore, the transient sources in third-octave bands on the turbine hub and blades were investigated and it was observed that they are not in an audible range. The inspection of the measurement angle showed the strong radiation pattern. When measuring from the left, the main emission was localised much higher than when measuring from the right. Last but not least, the comparison of the results between the measurements with the arrays Star48 and Fibonacci120 showed that the Star48-array has a good main lobe width but a poor dynamic. The main lobe width of the Fibonacci120 was also not very well, but this could be explained with the much smaller array aperture. Ideal case would be the design of the Fibonacci120 with the aperture of the Star48.

For the development of an approach for the investigation of sound emissions of wind turbines with acoustic cameras we can summarise that

- an integration time corresponding to one revolution shows us the location of the maximum sound emission,
- the upwind position leads to a little higher sound emission but the downwind position corresponding to the IEC-61400-11 standard [9] should be preferred (for a better comparability) and
- an array design with a spiral microphone arrangement and a big aperture leads to the best results.

Regarding to the investigation of the effectiveness of serrations it is a challenge to perform one measurements on a wind turbine with and another measurement on a turbine without serrations with exactly the same conditions (design of the wind turbine, weather conditions, measurement place, ...). The best approach would be to equip only one blade of a wind turbine with serrations or only one blade without serrations. This makes it possible to compare the sound emission of the different equipped blades with identical conditions during a measurement and could provide a quantitative statement.

6. REFERENCES

- [1] E. Pedersen and K. P. Waye, "Perception and annoyance due to wind turbine noise - a dose-response relationship," *J. Acoust. Soc. Am.*, vol. 116, pp. 3460–3470, 2004.
- [2] E. Pedersen, F. van den Berg, R. Bakker, and J. Bouma, "Response to noise from modern wind farms in the Netherlands," *J. Acoust. Soc. Am.*, vol. 126, pp. 634–643, 2009.
- [3] E. Koppen and K. Fowler, "International legislation for wind turbine noise," in *Proc. of Euro Noise 2015*, 2016.
- [4] O. Jaeckel, "Strengths and weaknesses of calculating beamforming in the time domain," in *Proc. of Berlin Beamforming Conference (BeBeC)*, 2006.
- [5] D. H. Johnson, *Array Signal Processing: Concepts and Techniques (Prentice-hall Signal Processing Series)*. Pearson Education (US), 1993.
- [6] E. Sarradj, "Optimal planar microphone array arrangements," in *Proc. of DAGA 2015*, 2014.
- [7] S. Wagner, R. Bareiß, and G. Guidati, *Wind Turbine Noise*. Springer Verlag, 1996.
- [8] M. Shibata, T. Furukawa, Y. Hayashi, and E. Kato, "Serrated wind turbine blade trailing edge," EUROPEAN PATENT APPLICATION EP 1 338 793 A3, Sep. 2010.
- [9] IEC, *Amendment 1 - Wind turbines - Part 11: Acoustic noise measurement techniques*. VDE Verlag, 2018.